SUPPLEMENTARY INFORMATION

Christopher J. Soelistyo[1,2] **Giulia Vallardi**[2] **Guillaume Charras**[1,3,4]

Alan R. Lowe[1,2,4,5*]

[1]Institute for the Physics of Living Systems
[2]Department of Structural and Molecular Biology
[3]Department of Cell and Developmental Biology
[4]London Centre for Nanotechnology
University College London, Gower St, London, WC1E 6BT, UK

[5]The Alan Turing Institute
Euston Rd, London NW1 2DB, UK

November 24, 2021

Contents

*To whom correspondence should be addressed: a.lowe@ucl.ac.uk

List of Figures

List of Tables

1 Additional methods

1.1 Cell culture

The MDCK cell lines used for this study scrib^{kd} were a kind gift from Prof Yasuyuki Fujita (University of Kyoto, Japan) and described in [1].To enable visualisation of nucleic acid organisation during the cell cycle, we established cell lines stably expressing fluorescently tagged histone markers. Use of different fluorescent proteins enabled us to distinguish the two competing cell types and allowed for accurate segmentation. MDCK^{WT} and scrib^{kd} cells expressing H2B-GFP and -RFP nuclear markers were described in [Bove et al, 2017]. All cell lines used in this publication have been tested for mycoplasma infection and were found to be negative (MycoAlert Plus Detection Kit, Lonza, LT07-710). MDCK cells were grown in DMEM (Thermo-Fisher) supplemented with 10% fetal bovine serum (FBS, Sigma-Aldrich), Hepes buffer (Sigma-Aldrich), and 1% Penicillin/Streptomycin in a humidified incubator at 37°C with 5% CO_2. The scrib^{kd} cells were cultured as wild-type cells, except that we used tetracycline-free bovine serum (Clontech, 631106) to supplement the culture medium. For inducing expression of scribble shRNA, doxycycline (Sigma-Aldrich, D9891-1G) was added to the medium at a final concentration of 1 μg/ml.

1.2 Automated Widefield Microscopy

A custom-built automated epifluorescence microscope was built inside a standard CO_2 incubator (Heraeus BL20) which maintained the temperature at 37°C and 5% CO_2. The microscope utilised an 20× air objective (Olympus Plan Fluorite, 0.5 NA, 2.1mm WD), high performance encoded motorized XY and focus motor stages (Prior H117E2IX, FB203E and ProScan III controller) and a 9.1MP CCD camera (Point Grey GS3-U3-91S6M). Brightfield illumination was provided by a fibre-coupled green LED (Thorlabs, 530nm). GFP and mCherry/RFP fluorescence excitation was provided by a LED light engine (Bluebox Optics niji). Cameras and light sources were synchronised using TTL pulses from an external D/A converter (Data Translation DT9834). Sample humidity was maintained using a custom built chamber humidifier. The microscope was controlled using MICRO-MANAGER [2] and our own software OCTOPUSLITE[2].

1.3 Cell competition assay

Cell competition assays were carried out in 24-well imaging plates (ibidi). At the start of each experiment, cells were seeded at an initial density of 1×10^{-3} cells/μm^2. MDCK^{WT} cells expressing H2B-GFP were mixed with scrib^{kd} H2B-RFP cells at a ratio of 90:10, 50:50 or 10:90. In some experiments, the expression of scribble shRNA was been induced in scrib^{kd} cells by exposure to 1ug/mL doxycycline for 70 hours before seeding. In other experiments, the cells were maintained in tetracycline free medium to prevent scribble shRNA induction. Imaging was started 2–3 h after seeding. Imaging medium used during the assay was phenol red free DMEM (Thermo Fisher Scientific, 31053) supplemented with tetracycline-free bovine serum, Hepes, antibiotics and, for experiments involving induction, doxycycline at the dose indicated above. Multi-location imaging was performed inside the incubator-scope acquiring Bbrightfield, GFP and RFP fluorescence images with a frequency of 1 frame every 4 minutes for each position for 80 hours (1200 frames).

1.4 Image alignment and normalization

Image stacks were aligned using StackReg [3]. All images used in the analysis were normalized to have a mean value of zero and unit variance.

1.5 Single cell tracking

Instance segmentation of individual cells in timelapse microscopy sequences was performed using a residual U-Net as previously described. We used a Bayesian cell tracking approach[3] to assemble single-cell cell trajectories from the data [4, 5].

1.6 Glimpse extraction, cell fate classification and determination of cutoff

Glimpses are extracted at 64×64, 128×128 and 256×256 pixels, centred on the cell of interest at each time point, and downsampled to 64×64 pixels. We use the first scale as input to the trajectory classification network, reasoning that the morphology of the nucleus is sufficient to classify the fate of the cell. We trained a combined CNN-LSTM

[2] `https://www.github.com/quantumjot/octopuslite`

[3] `https://www.github.com/quantumjot/bayesiantracker`

neural network to classify each trajectory as containing either a mitotic or an apoptotic event. This network was trained using 7,922 manually labelled trajectories: 4,401 mitoses, 828 apoptoses and 2,693 "unknown" trajectories. The latter refers to trajectories in which neither a mitosis nor an apoptosis occurs. The CNN and the LSTM [6] were trained separately. The CNN was trained to classify individual fluorescence images according to the morphological state of the nucleus ("interphase", "metaphase", "prometaphase", "anaphase" or "apoptotic") [4, 5]. The LSTM was trained to integrate the time-specific state classifications in a trajectory to arrive at a classification of the trajectory as a whole ("mitotic", "apoptotic" or "unknown"). Trajectories terminating with an unknown classification arise when a cell exits the microscope's field of view (FOV) or the movie terminates before an event can occur.

Various augmentation techniques were used to train both the CNN and the LSTM. For the CNN, we used random flipping, cropping, rotation, translation, noise addition, brightness adjustment, and aspect ratio adjustment on the training images. For the LSTM, we used frame-swapping, random-frame-deletion and noise addition on the training trajectories. After all of the labelled trajectories were obtained, an automated procedure was applied to shorten the duration of the glimpses so as to leave out the portion of each time-series that contains the fate event (the mitosis or apoptosis event) (**Fig S4**). This pruning procedure ensured that the prediction network could not use morphological changes arising as a consequence of cell fate.

1.7 Confusion matrices

To assess the classification performance of our networks, we computed a confusion matrix. In a confusion matrix, the number in row i and column i represents the number of data instances in the testing set that are of ground-truth class i yet are classified as belonging to class j by the model. We often used a normalized confusion matrix, where each element in row i is written as a proportion of the sum of elements in row j (i.e. the number of ground-truth examples of class j).

1.8 Cell masking procedure

We performed cell masking as follows. First, we used the U-Net segmentation of our glimpse images to find the regions in each image that corresponded to cells, and conversely, the regions that corresponded to the background. Next, we identified the cell-regions that corresponded to either the central cell, or the cells in the neighbourhood, depending on which we wished to mask. In the "Mid-View, Central Cell Only" framework, we masked the neighbourhood cells, whereas in the "Mid-View, Neighbour Cells Only" framework we masked the central cell. Finally, we calculated the mean and standard deviation of pixel values in the background region, and then used these values to replace the masked region with Gaussian noise, such that this region appears similar to the background.

1.9 Calculation of image properties and correlation with principal components

To calculate image properties, we used scikit-image regionprops. We calculated the following properties for the central cell of each glimpse using the intensity images and the U-Net segmentation:

- `area`
- `eccentricity`
- `orientation`
- `solidity`
- `intensity_mean`

Separately, we also calculated the number of cells by counting the number of unique connected components in the U-Net binary segmentation of the glimpse, using the `label` function from the `morphology` module of scikit-image. The aspect ratio of the cells was calculated by finding the ratio between the maximum horizontal and vertical spans of the cells as given by their U-Net segmentations.

1.10 Computational hardware

All code was implemented in Python and C/C++ using CVXOPT, GLPK, Numpy, Scipy, Scikit-Image, Scikit-Learn, TensorFlow, Keras and JAX libraries. Microscopy image visualisation was performed using NAPARI[7]. All image processing was performed on a ASUS ESC4000 G3 server (RackServers.com) running Ubuntu 18.04 LTS with 256Gb RAM and NVIDIA GTX1080 Ti or V100 GPUs.

2 Supplementary figures

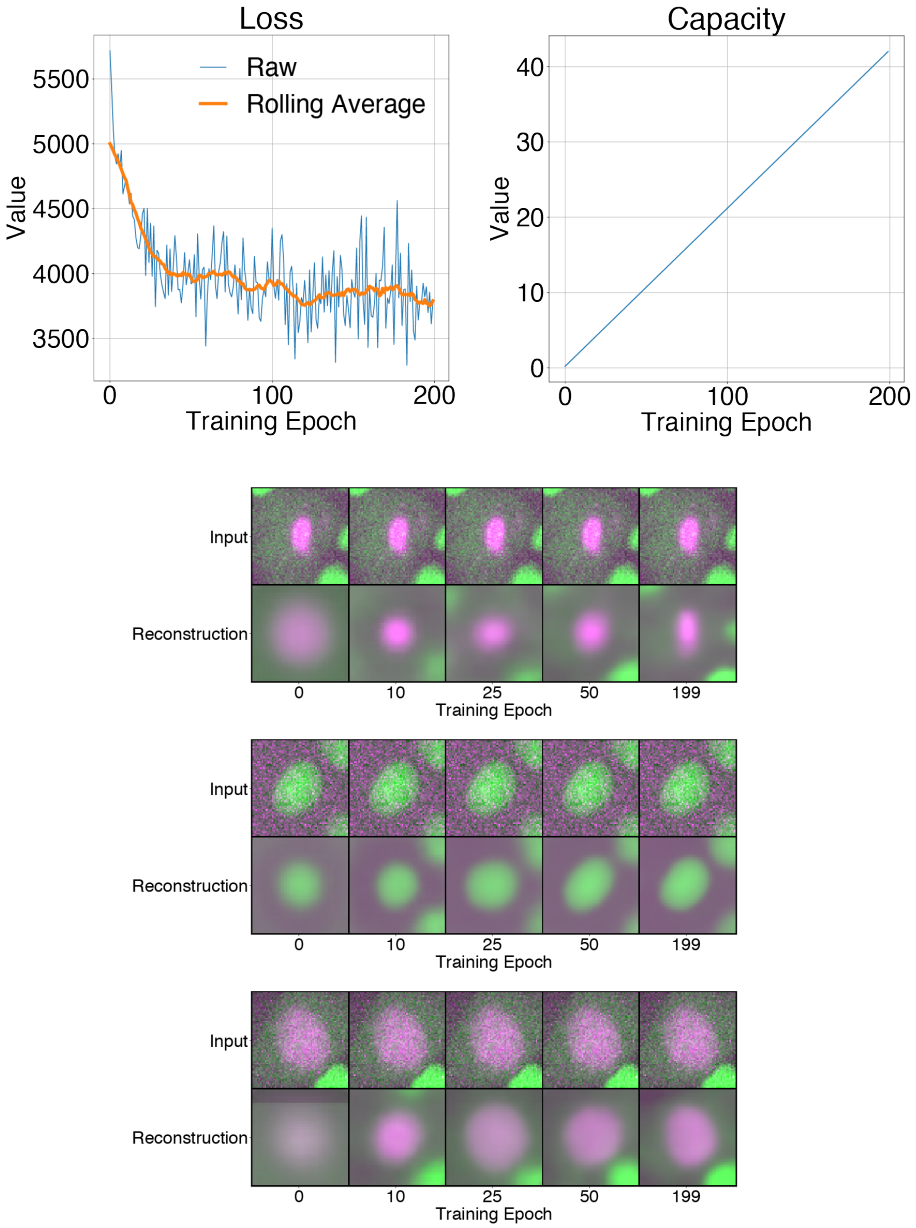

Figure 1: **Example of linear increase of β-VAE bottleneck capacity during training.** (a) Decreasing loss as a function of training iteration. (b) Linear increase in bottleneck capacity during training (d) Example images generated by sampling during training, demonstrating the acquisition of fine details as capacity increases.

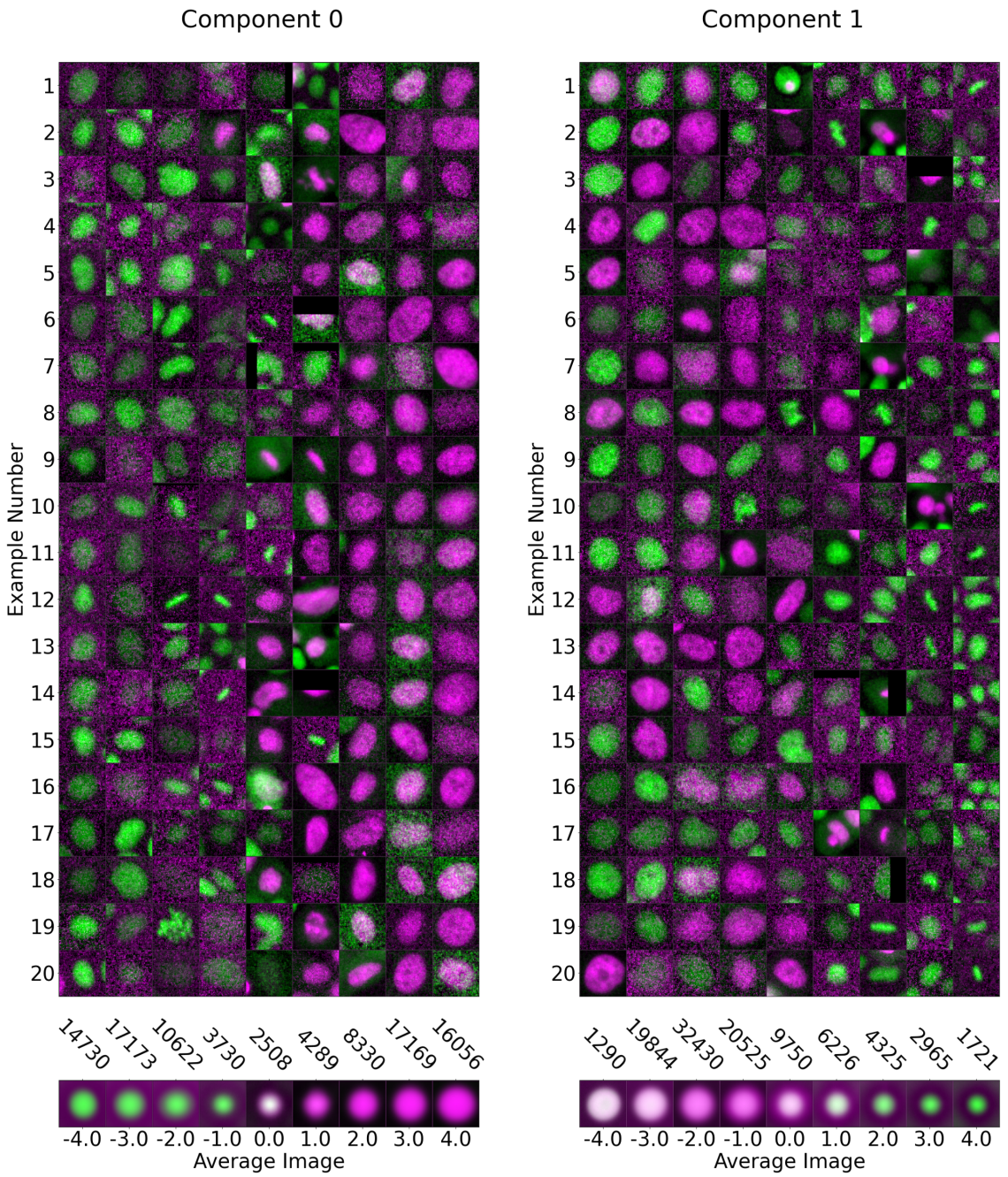

Figure 2: **Graded examples of PC0 and PC1.** This figure displays some example cell fluorescence images that correspond to certain values of PC0 and PC1. For each component value $V = -4.0, 3.0, ..., 4.0$, twenty images have been shown for whom their associated PC0 or PC1 value v falls within the range $V - 0.5 < v < V + 0.5$. The sub-figure below shows the resulting "average image" obtained by taking the mean of every image in a 100,000-image dataset that corresponds to the aforementioned PC-value ranges. The number above each average image represents the number of raw images that have been averaged to obtain it. As can be seen, PC0 correlates strongly with cell type, whereas PC1 correlates strongly with cell density/nuclear size. The PC1/cell-type correlation can perhaps be explained by the fact that the nuclei of scrib^{kd}cells tend to be larger, therefore there are few scrib^{kd}cells at high values of PC1. Additionally, there are relatively few examples of scrib^{kd} cells at very high density, due to the competition itself.

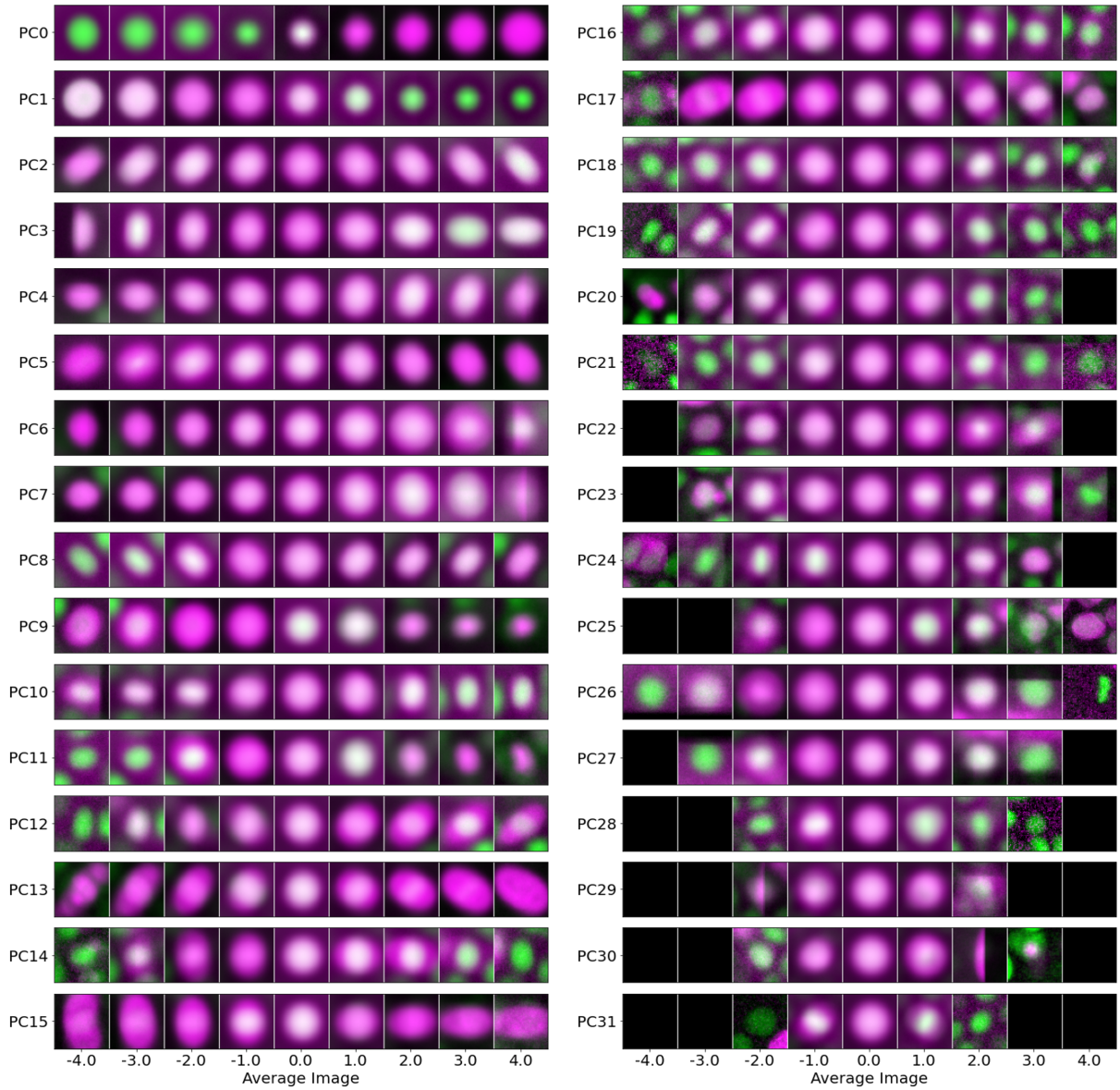

Figure 3: **Examples of all Principal Components.** After PCA was applied to the latent space, it was found that several of the principal components corresponded to interpretable features of the cell fluorescence images. This figure portrays the result of taking the mean of all images from a dataset of 100,000 images whose corresponding value of a particular principal component fell within a specific range (the x-axis value ± 0.5). What is obtained is a way of visualising how the images differ with the variation of any one principal component. This visualisation is shown for all thirty-two principal components extracted using PCA. It can seen that, for example, PC0 corresponds primarily to cell type, whereas PC1 corresponds to cell density/nuclear area, PC5 to orientation, PC3 to aspect ratio, and so on. At the extremities of the plotted range, images may appear to be atypically detailed. This is due to the paucity of image examples that correspond to very high or low values of a particular principal component.

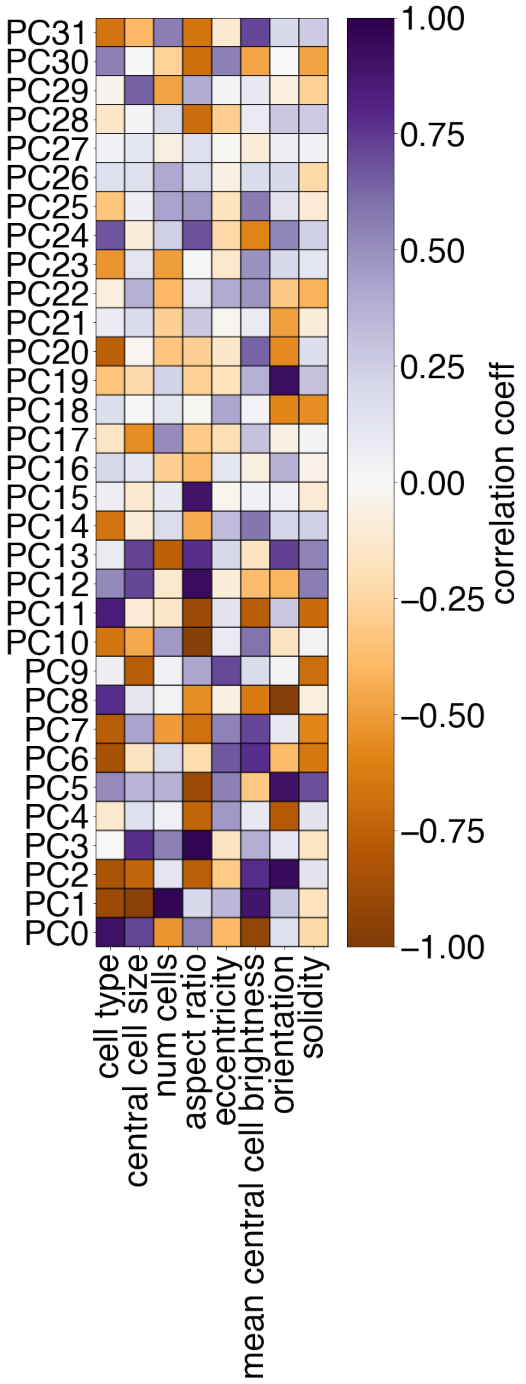

Figure 4: **Correlation of all Principal Components with measureable parameters.** This figure shows the correlation coefficients of all the Principal Components with certain calculated variables. These variables were calculated based on the intensity images of example cell crops and their associated U-Net segmentations (see Section 1.9 for more details). The results shown here can be cross-referenced with the results shown in Figure 3 to arrive at an interpretation of the physical features to which the Principal Components correspond.

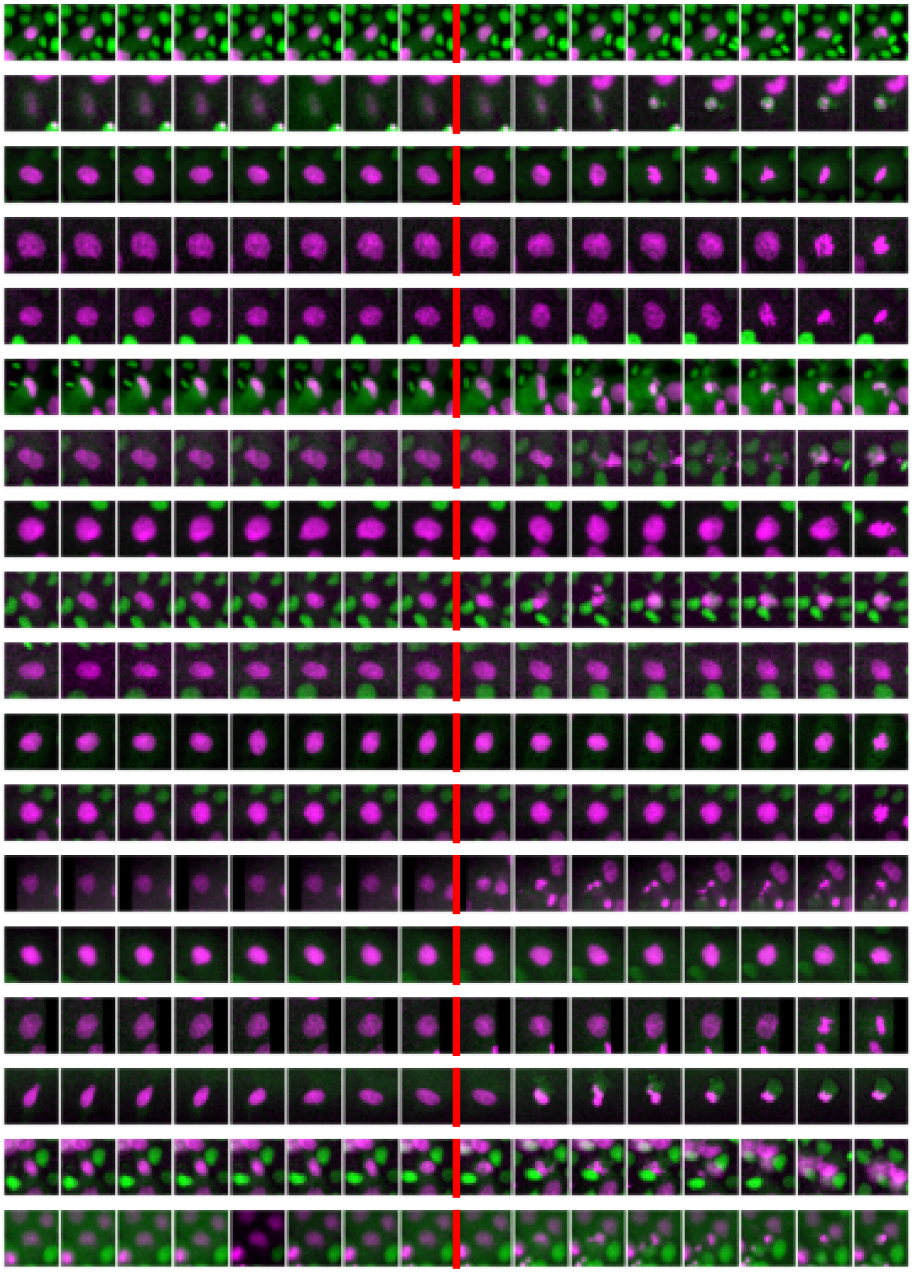

Figure 5: **Example scrib^{kd}trajectories.** Each trajectory is cropped to $\pm$ 32 minutes around the cutoff (red vertical line). The cutoff represents the point after which there are visible changes to the chromatin morphology which signify either apoptosis or mitosis.

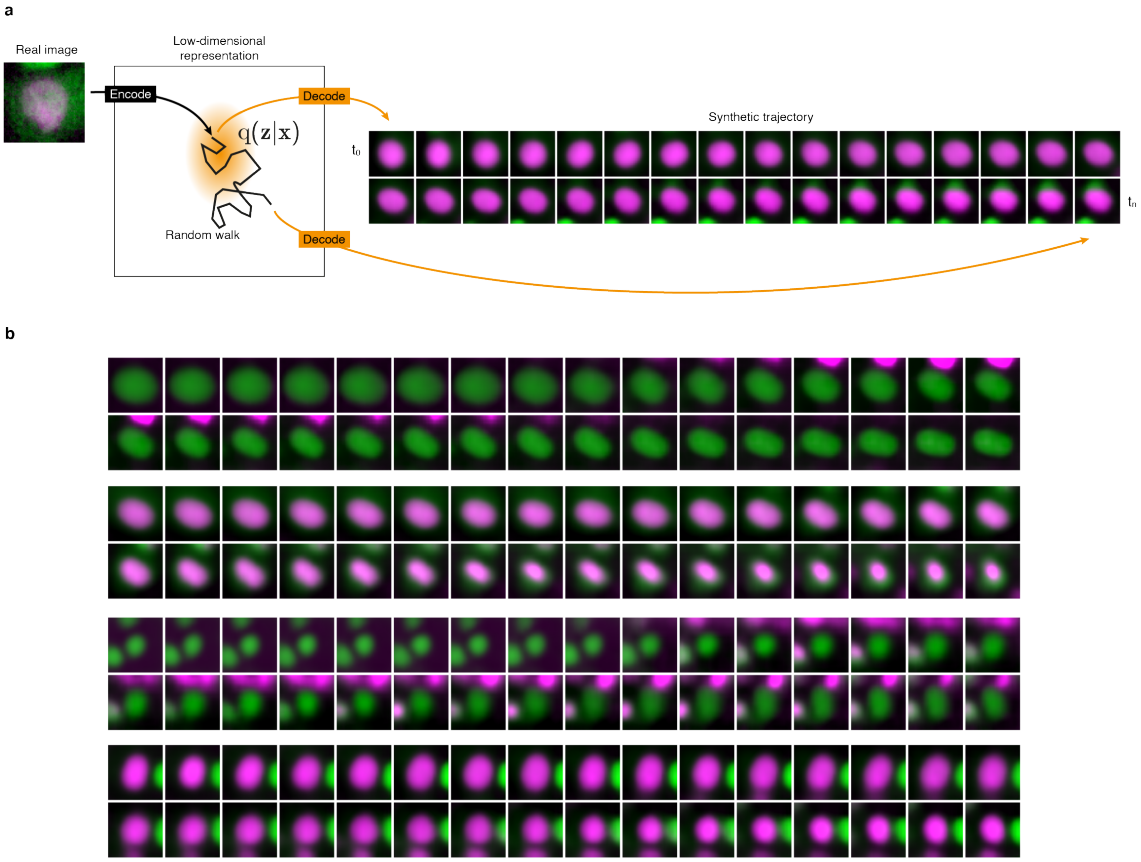

Figure 6: **Generative modeling of "synthetic" trajectories.** (a) For each synthetic trajectory we start by encoding a real image as a starting point. Next, we take a random walk in the latent space. These trajectories in latent space are used as inputs to the TCN. Here, we also use the decoder to generate image sequences that represent the random walks in latent space. (b) Four example synthetic trajectories.

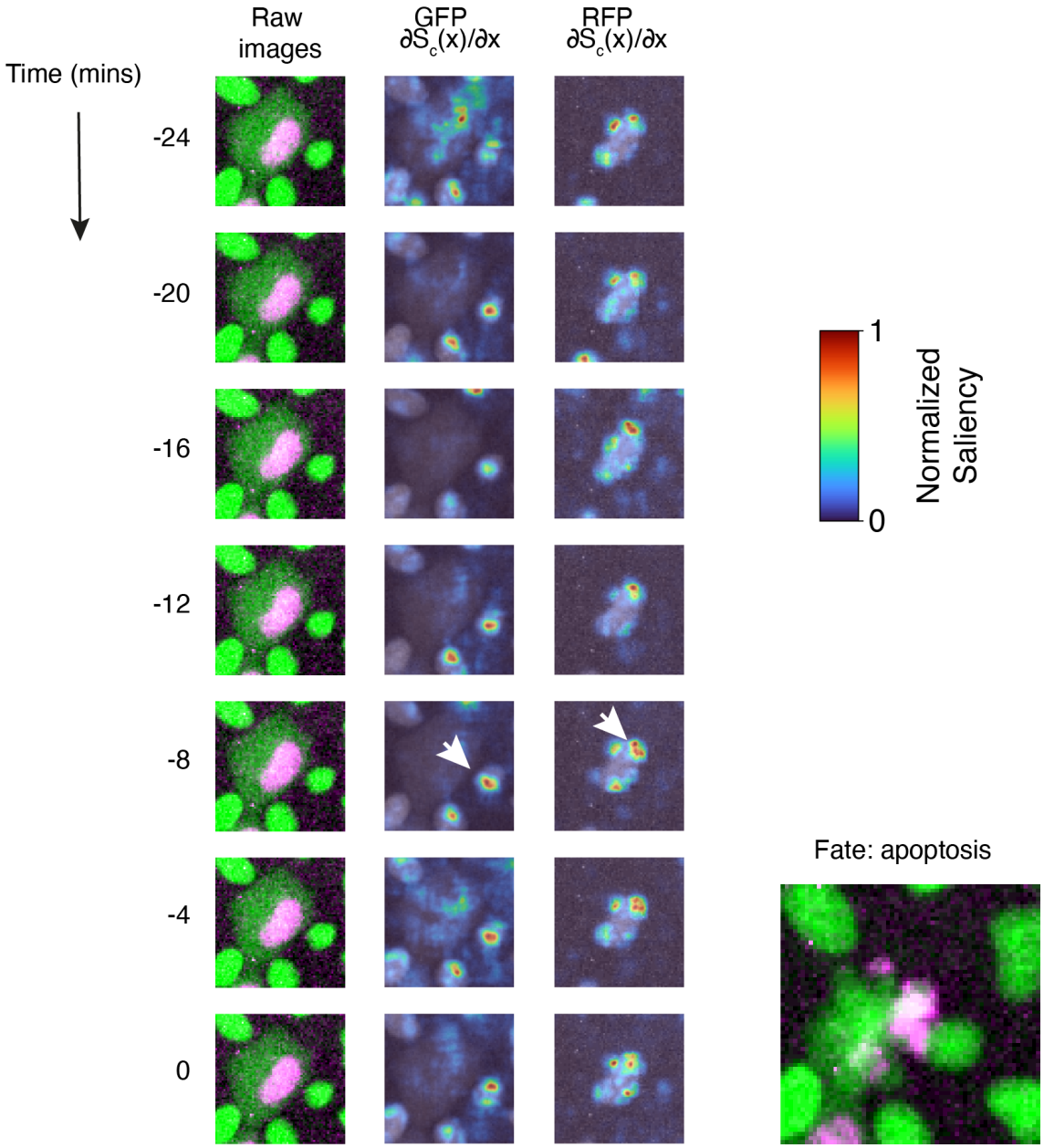

Figure 7: **Example of a feature saliency heatmaps for a scrib^{kd} apoptosis event.** Here we calculate the feature saliency w.r.t. the input pixel data by backpropagating through the TCN and the convolutional encoder of the β-VAE. The input image data is shown in the left column. The middle column shows pixel saliency in the GFP channel of the input. The right column shows pixel saliency in the RFP channel of the input. Each image of the saliency is normalized per time point. Large gradient magnitudes (reds, yellows) indicate higher feature saliency. White arrows at indicate examples of regions of high saliency corresponding to nearby dividing cells or changes in the nuclear morphology of the target cell.

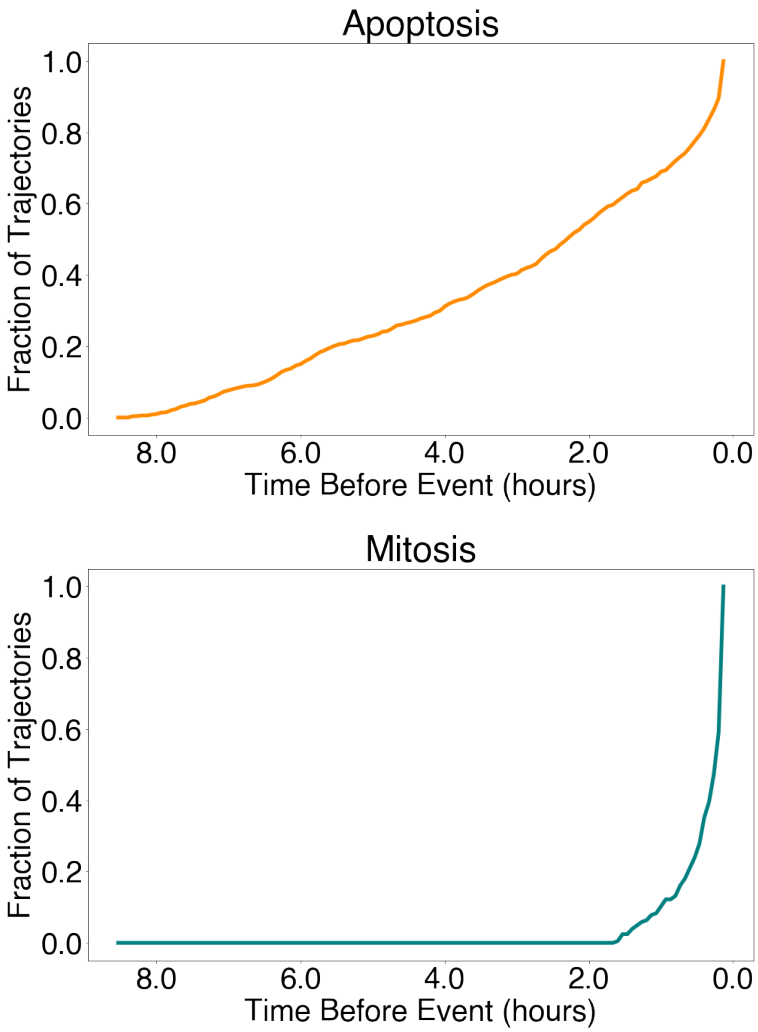

Figure 8: **Fraction of correct predictions at different timescales for scrib^{kd} cells.** After being fed a given number of frames of input, the TCN assigns a final-layer logit value to each label (apoptosis, mitosis or synthetic), which, after application of the softmax activation function, can be taken as the "confidence" value of the TCN in any particular label. In general, as the TCN is fed consecutive frames, it becomes gradually more confident in the correct prediction. This figure is based on a set of trajectories for which all of the trajectories were classified correctly by the TCN with at least 99% confidence (a threshold of $T = 0.99$) after the TCN was fed every frame of the trajectory. It shows how the fraction of trajectories classified correctly with a threshold of $T = 0.99$ increases as the length of input increases. These data can potentially be used to determine the common length of input required before the TCN becomes confident in any particular cell fate.

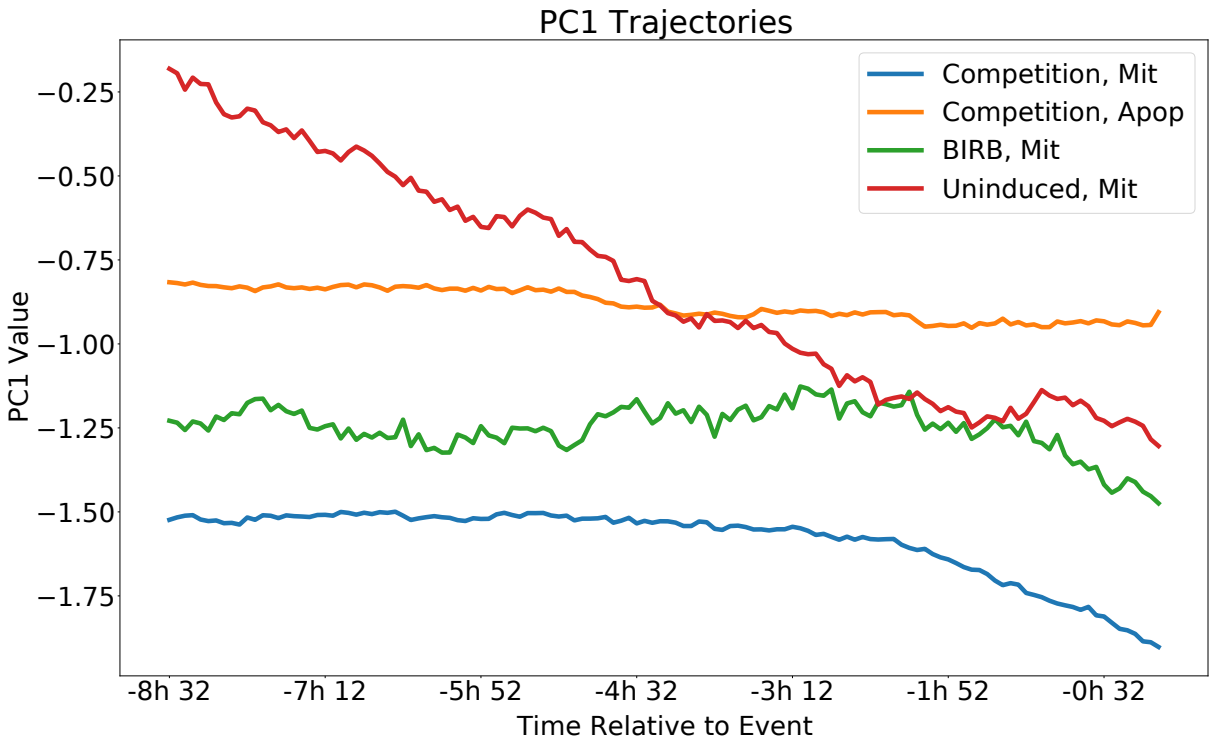

Figure 9: **PC1 trajectories.** This figure shows the result of collecting all of the scrib^{kd}cell trajectories that were labelled 'apoptosis' or 'mitosis' (by the trajectory-classification network, in the case of the mitoses, and manually, in the case of the apoptoses) and then finding the average value over time of PC1, which correlates strongly with cell size/cell density. This was done for the "Competition", "BIRB" and "Uninduced" conditions. Some patterns emerge from these plots. The first is that there tends to be a drop in PC1 in the run-up to a mitosis event; this is consistent across all the drug treatments used. The second is that PC1 tends to be higher for apoptoses throughout the trajectory, in comparison to mitoses. Interestingly, the mean PC1 values tended to be higher in mitoses from the BIRB and Uninduced datasets, compared to the Competition dataset. This suggests that in the BIRB and Uninduced datasets, the scrib^{kd}cells displayed a higher tolerance to compaction compared to the Competition dataset (i.e. they could be subjected to higher levels of compaction and still divide rather than apoptose). This is consistent with the known role of p38 kinase in stress response pathways activated by mechanical competition and the lack of competition when scribble knock down is not induced. (Supplementary Table 3). Similar effects can be observed in the confusion matrices obtained for these conditions (see main text).

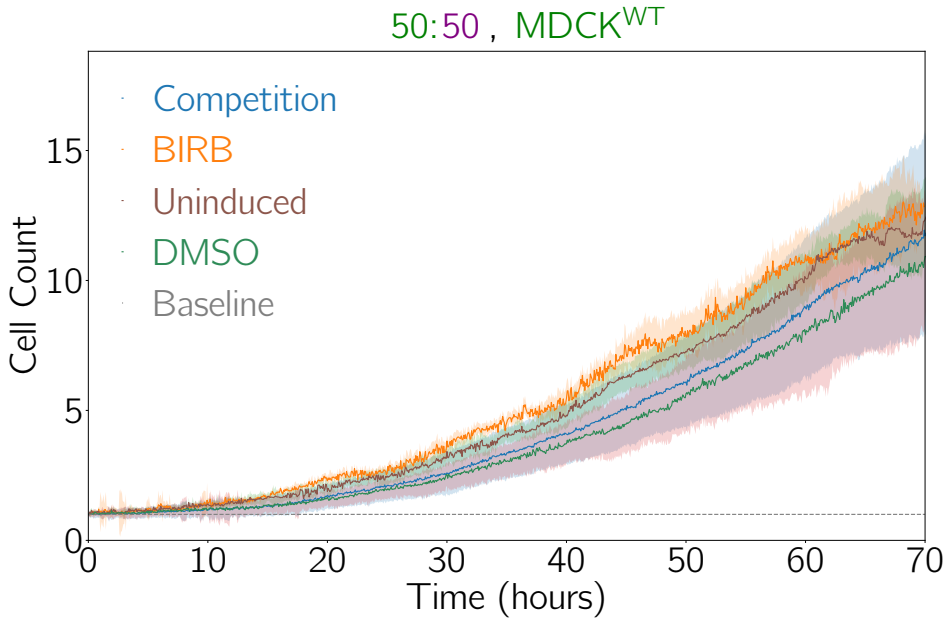

Figure 10: **Normalized cell counts for MDCK^{WT} cells under various conditions.** "Competition" (cell competition between MDCK^{WT} and scrib^{kd} cells), "BIRB" (competition in the presence of BIRB796), "Uninduced" (where the scrib^{kd} cells are uninduced and therefore neither knock-down nor competition occur), and "DMSO" (competition in the presence of dimethyl sulfoxide). Since DMSO was used as a negative control, it was expected that the "DMSO" and "Competition" conditions would produce similar cell count plots. The ratio of MDCK^{WT} to scrib^{kd} cells at the beginning of the experiments was prepared to be 50:50. The cell counts have been normalized relative to the initial count at the beginning of the experiment. This initial level is represented by the "Baseline" plot.

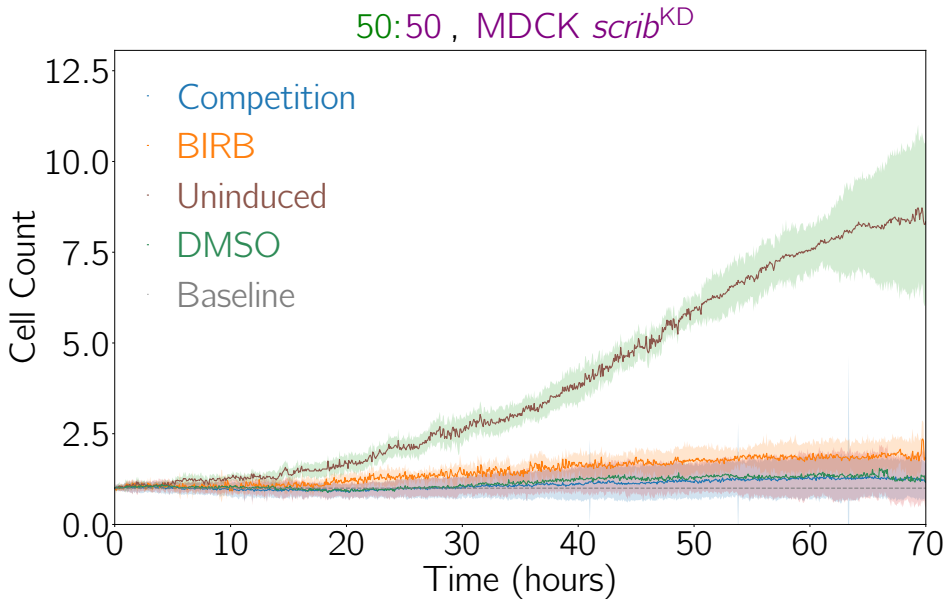

Figure 11: **Normalized cell counts for scrib^{kd} cells under various conditions.** In the "Uninduced" plot, where Scribble knock-down does not occur, the cell count follows a trajectory not too dissimilar to that which MDCK^{WT} cells would take. However, in the "Competition" plot, the cell count remains close to the Baseline, reflecting the inhibition of scrib^{kd} population growth as a result of apoptosis induced by cell competition. The "BIRB" plot shows how scrib^{kd} population growth is affected by treatment of BIRB796, which prevents apoptosis by inhibiting the p38 kinase stress response pathways activated by competition. The result is that population growth is higher, though not to same extent as when competition is wholly absent. Finally, the "DMSO" plot follows very closely the trajectory taken by the "Competition" plot, which is to be expected, since DMSO was used as a negative drug control.

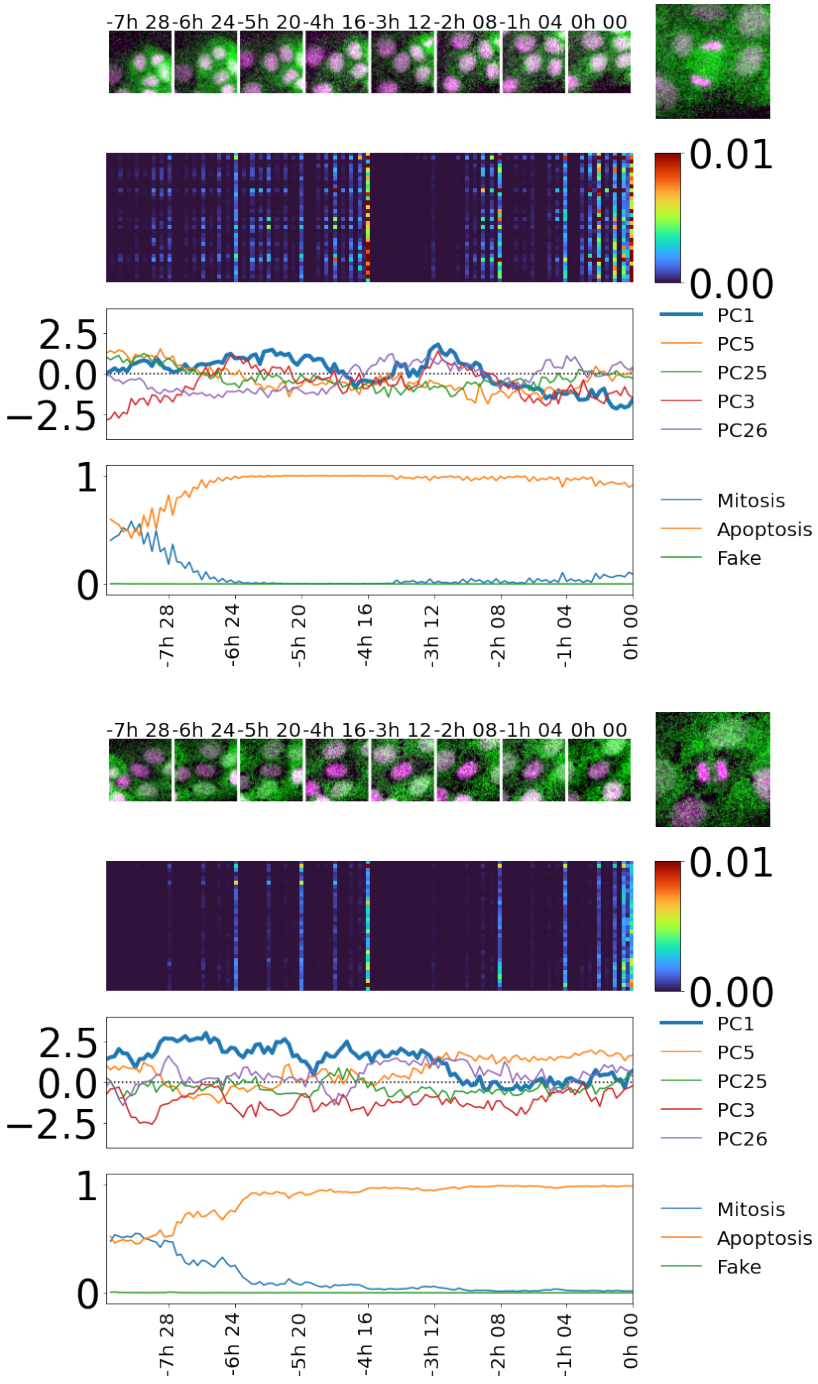

Figure 12: **Example incorrect predictions of cell fate in the uninduced (scrib$^{kd,\ tet-}$) dataset.** Two example trajectories are shown, with one sub-figure for each. At the top of each sub-figure is placed a collage of time-points of the trajectory before the "cutoff" point. To the right is the final time-point of the trajectory (after the cutoff point), revealing the cell fate. Below that is shown, in order: the confidence plot, showing the TCN's predictions over time; a plot of PC1, the most important principal component for fate prediction; a saliency heat-map showing which components were most important to the prediction, and when and; a saliency plot over time for PC1. In both cases, a ground-truth mitosis was classified by the TCN to be apoptotic; presumably because of the high PC1 recorded (high density) throughout the trajectory. This error could be interpreted as arising due to the fact that in the Uninduced dataset, Scribble knock-down does not occur, and therefore, competition does not occur. As a result, scrib^{kd}cells could endure high densities that would have been fatal for them under conditions of competition.

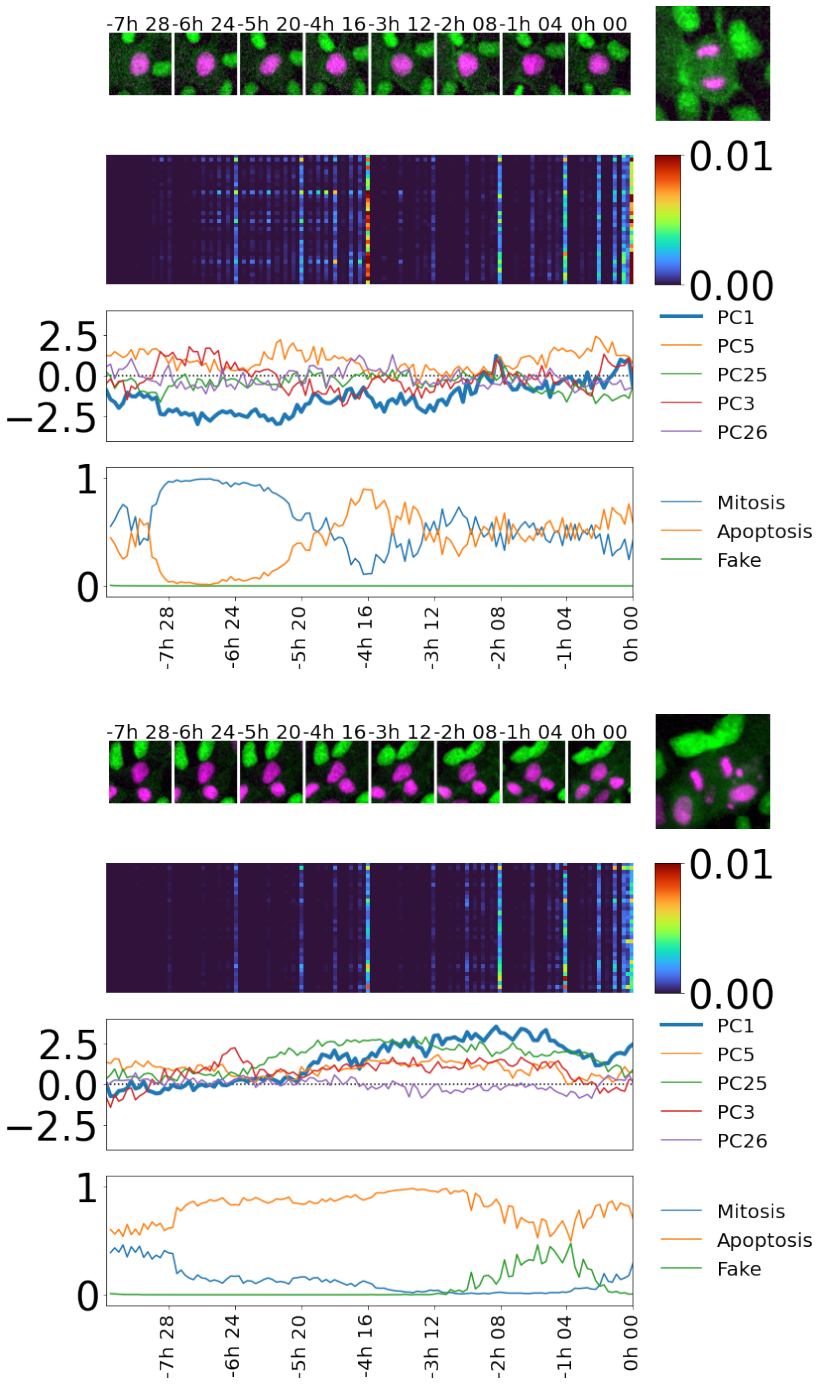

Figure 13: **Example incorrect predictions of cell fate in the BIRB796 treated dataset.** Two example trajectories are shown, with one sub-figure for each. At the top of each sub-figure is placed a collage of time-points of the trajectory before the "cutoff" point. To the right is the final time-point of the trajectory (after the cutoff point), revealing the cell fate. Below that is shown, in order: the confidence plot, showing the TCN's predictions over time; a plot of PC1, the most important principal component for fate prediction; a saliency heat-map showing which components were most important to the prediction, and when and; a saliency plot over time for PC1. In both cases, a ground-truth mitosis was classified by the TCN to be apoptotic; presumably because of the high PC1 (high density) recorded throughout the trajectory. This error could be interpreted as arising due to the fact that BIRB796 inhibits the p38 kinase stress response pathways that trigger apoptosis as a result of competition. With these pathways inhibited, cells that would otherwise have apoptosed instead divide.

3 Supplementary tables

Table 1: Datasets used in this study. All movies were captured with a size 1600×1200 pixels (corresponding to $530 \times 400\,\mu m$) with 3 channels (Brightfield, GFP and RFP).

Drug treatment	Cell types			Movies	Images
	GFP	RFP	Seeding Ratio		
None	$MDCK^{WT}$	$scrib^{kd}$	90:10	23	23,521
	$MDCK^{WT}$	$scrib^{kd}$	50:50	62	66,607
	$MDCK^{WT}$	$scrib^{kd}$	10:90	26	26,386
Uninduced	$MDCK^{WT}$	$scrib^{kd, tet-}$	50:50	6	5,925
	$MDCK^{WT}$	$scrib^{kd, tet-}$	10:90	5	5,814
BIRB796	$MDCK^{WT}$	$scrib^{kd}$	50:50	5	5,108
Total				127	133,361

Table 2: Single-cell trajectory training datasets used in this study. († see Methods)

Fate	$MDCK^{WT}$	$scrib^{kd}$	Total
Apoptotic	384	1841	2,225
Mitotic	34813	1249	36,062
Fake	Dynamically generated†		
Total	35197	3090	38287

Table 3: Drugs used in this study

Name	Biochemical activity	Concentration (μM)	Reference
BIRB796	p38 kinase inhibitor	2	[8]
DMSO	control	-	

Table 4: The testing macro-F1 of trained TCNs using various VAE models.

Model	$MDCK^{WT}$	$scrib^{kd}$	Average	Rank
Small-View, All Cells	91 ± 3%	84 ± 3%	87 ± 2%	1
Mid-View, Central Cell Only	90 ± 3%	85 ± 4%	87 ± 2%	2
Mid-View, All Cells	81 ± 3%	75 ± 4%	78 ± 2%	3
Mid-View, Neighbour Cells Only	78 ± 3%	74 ± 4%	76 ± 3%	4
Large-View, All Cells	76 ± 3%	65 ± 5%	70 ± 3%	5

4 Supplementary movies

4.1 Movie S1

Timelapse acquistion and tracking of single cell, showing three different spatial scales extracted to form the glimpse.

4.2 Movie S2

Glimpse extracted from movie S1.

4.3 Movie S3

Example cell detection and tracking for MDCK$^{\mathrm{WT}}$:scrib$^{\mathrm{kd}}$ dataset.

4.4 Movie S4

Example cell detection and tracking for MDCK$^{\mathrm{WT}}$:scrib$^{\mathrm{kd,\ tet\text{-}}}$ dataset.

4.5 Movie S5

Example cell detection and tracking for MDCK$^{\mathrm{WT}}$:scrib$^{\mathrm{kd}}$ + 2 µM BIRB796 dataset.

4.6 Movie S6

Example τ-VAE output for MDCK$^{\mathrm{WT}}$:scrib$^{\mathrm{kd}}$ dataset.

4.7 Movie S7

Example τ-VAE output for MDCK$^{\mathrm{WT}}$:scrib$^{\mathrm{kd,\ tet\text{-}}}$ dataset.

4.8 Movie S8

Example τ-VAE output for MDCK$^{\mathrm{WT}}$:scrib$^{\mathrm{kd}}$ + 2 µM BIRB796 dataset.

References

[1] M. Norman, K. A. Wisniewska, K. Lawrenson, P. Garcia-Miranda, M. Tada, M. Kajita, H. Mano, S. Ishikawa, M. Ikegawa, T. Shimada, and Y. Fujita, "Loss of scribble causes cell competition in mammalian cells," *Journal of Cell Science*, vol. 125, no. 1, pp. 59–66, 2012.

[2] A. D. Edelstein, M. A. Tsuchida, N. Amodaj, H. Pinkard, R. D. Vale, and N. Stuurman, "Advanced methods of microscope control using μmanager software," *Journal of Biological Methods*, vol. 1, p. e10, Nov. 2014.

[3] P. Thévenaz, U. Ruttimann, and M. Unser, "A pyramid approach to subpixel registration based on intensity," *IEEE Transactions on Image Processing*, vol. 7, pp. 27–41, January 1998.

[4] A. Bove, D. Gradeci, Y. Fujita, S. Banerjee, G. Charras, and A. R. Lowe, "Local cellular neighborhood controls proliferation in cell competition," *Molecular Biology of the Cell*, vol. 28, no. 23, pp. 3215–3228, 2017. PMID: 28931601.

[5] K. Ulicna, G. Vallardi, G. Charras, and A. R. Lowe, "Automated deep lineage tree analysis using a Bayesian single cell tracking approach," *Frontiers in Computer Science*, sep 2021.

[6] S. Hochreiter and J. Schmidhuber, "Long short-term memory," *Neural Computation*, vol. 9, no. 8, pp. 1735–1780, 1997.

[7] N. Sofroniew, T. Lambert, K. Evans, J. Nunez-Iglesias, P. Winston, G. Bokota, K. Yamauchi, A. C. Solak, ziyangczi, G. Buckley, M. Bussonnier, G. Peña-Castellanos, D. D. Pop, Pam, T. Tung, V. Hilsenstein, alisterburt, Hector, J. Freeman, P. Boone, A. R. Lowe, C. Gohlke, L. Royer, kir0ul, H. Har-Gil, M. Kittisopikul, S. Axelrod, A. Patil, A. McGovern, and A. Rokem, "napari/napari: 0.4.7rc1," Mar. 2021.

[8] Y. Kuma, G. Sabio, J. Bain, N. Shpiro, R. Márquez, and A. Cuenda, "BIRB796 inhibits all p38 MAPK isoforms in vitro and in vivo," *Journal of Biological Chemistry*, vol. 280, pp. 19472–19479, may 2005.